Vol. 427: 29–49, 2011
doi: 10.3354/meps09043

MARINE ECOLOGY PROGRESS SERIES
Mar Ecol Prog Ser

Published April 12

Effects of surface forcing on interannual variability of the fall phytoplankton bloom in the Gulf of Maine revealed using a process-oriented model

Song Hu[1,*], Changsheng Chen[1,2], Rubao Ji[1,3], David W. Townsend[4], Rucheng Tian[2], Robert C. Beardsley[5], Cabell S. Davis[3]

[1]Marine Ecosystem and Environmental Laboratory, College of Marine Sciences, Shanghai Ocean University, 999 Hucheng Huanlu, Lingang New City, Shanghai 201306, PR China

[2]School for Marine Science and Technology, University of Massachusetts Dartmouth, 706 South Rodney French Blvd., New Bedford, Massachusetts 02744, USA

[3]Department of Biology, Woods Hole Oceanographic Institution, Woods Hole, Massachusetts 02543, USA

[4]School of Marine Sciences, University of Maine, 5706 Aubert Hall, Orono, Maine 04469, USA

[5]Department of Physical Oceanography, Woods Hole Oceanographic Institution, Woods Hole, Massachusetts 02543, USA

ABSTRACT: SeaWiFS (Sea-viewing Wide Field-of-view Sensor) chlorophyll data revealed strong interannual variability in fall phytoplankton dynamics in the Gulf of Maine, with 3 general features in any one year: (1) rapid chlorophyll increases in response to storm events in fall; (2) gradual chlorophyll increases in response to seasonal wind- and cooling-induced mixing that gradually deepens the mixed layer; and (3) the absence of any observable fall bloom. We applied a mixed-layer box model and a 1-dimensional physical-biological numerical model to examine the influence of physical forcing (surface wind, heat flux, and freshening) on the mixed-layer dynamics and its impact on the entrainment of deep-water nutrients and thus on the appearance of fall bloom. The model results suggest that during early fall, the surface mixed-layer depth is controlled by both wind- and cooling-induced mixing. Strong interannual variability in mixed-layer depth has a direct impact on short- and long-term vertical nutrient fluxes and thus the fall bloom. Phytoplankton concentrations over time are sensitive to initial pre-bloom profiles of nutrients. The strength of the initial stratification can affect the modeled phytoplankton concentration, while the timing of intermittent freshening events is related to the significant interannual variability of fall blooms.

KEY WORDS: Fall phytoplankton bloom · Surface forcing · Freshening · Interannual variability · Gulf of Maine · Modeling

INTRODUCTION

The Gulf of Maine (GoM) is a semi-enclosed continental shelf system located in the Northwest Atlantic (see Fig. 1). The biological oceanography of the GoM is dominated by prominent spring phytoplankton blooms that have been studied extensively since the pioneering work of Bigelow (1926) and Gran & Braarud (1935). Later studies have continued to focus on spring phytoplankton dynamics in the Gulf (e.g. Hitchcock & Smayda 1977a,b, Townsend & Spinrad 1986, Townsend et al. 1992, 1994, Thomas et al. 2003, Ji et al. 2006, 2008a,b), but far less attention has been paid to the fall bloom until recently. The spring bloom, in general, results from increasing light and seasonal stratification, at a time when the water column is replete with nutrients. The relatively weak bloom in fall (O'Reilly & Busch 1984, Thomas et al. 2003) occurs in the stratified season in response to increased vertical mixing that sufficiently erodes the stratification to mix

*Email: shu@shou.edu.cn

deep nutrients into the upper water column, where light is not limiting. While the fall bloom is mainly composed of the smaller-sized phytoplankton groups (dinoflagellates) (O'Reilly & Busch 1984) rather than larger diatoms that are common in the spring bloom, the importance of the fall bloom to overall ecosystem structure and function can be significant. Greene & Pershing (2007) have speculated that climate change-induced freshening at higher latitudes could enhance downstream phytoplankton blooms in the fall, which, in turn, could affect zooplankton dynamics in the region. The interannual variability of the fall bloom might also have important implications for populations at higher trophic level. For instance, Friedland et al. (2008) linked the fall bloom to haddock recruitment on Georges Bank, arguing that the intensity of the fall bloom influences maternal well-being and egg viability the following spring, although the detailed mechanisms remain to be further examined.

Our key question here is: What are the mechanisms and physical-biological dynamics controlling the interannual variability of fall phytoplankton blooms? If, for example, the erosion of stratification and the concomitant nutrient flux are the triggers of the bloom, one would expect that both local forcing (such as wind and cooling) and remotely controlled surface freshening can result in interannual variations in phytoplankton development. This can be modified further by storm events that can bring nutrients from the deeper layers to the euphotic zone and stimulate episodic phytoplankton blooms. Such events have been observed in the South Atlantic Bight, in the Gulf Stream (Fogel et al. 1999), and in the shelf and offshore regions of Nova Scotia and Newfoundland, Canada (Son et al. 2007). It remains unclear, however, to what extent those short-term events (versus gradual seasonal mixing) contribute to overall fall bloom dynamics.

In this study, we use modeling approaches to identify and understand the impacts of surface forcing on the interannual variability of fall phytoplankton blooms. First, we summarize the interannual variability of surface phytoplankton concentrations at the center of Wilkinson Basin in the GoM (see Fig. 1) in fall based on SeaWiFS (Sea-viewing Wide Field-of-view Sensor) remote sensing data. Then, we use a mixed-layer box model and a 1-dimensional (1D) coupled physical-biological model to analyze the responses of fall blooms to the physical forcing.

In the box-model approach, we simplified the physical mixing process by using time sequences of pre-calculated mixed-layer depths to estimate the flux of nutrients and its impact on other biological compartments. In the 1D approach, we conducted a series of numerical experiments in a vertical physical-biological model by using various values of wind stress, heat flux, and freshening. The advantage of the 1D model is the ability to include more detailed mixing processes explicitly than the box model. The physical model is the finite-volume community ocean model (FVCOM) with a 1D configuration. The biological model describes a simple NPZD (nitrate, phytoplankton, zooplankton, and detritus) lower-trophic food web dynamic. In order to better understand the role of each biological compartment, we conducted simulations sequentially starting with an N model, to an NP model, followed by an NPZ model and an NPZD model.

METHODS

SeaWiFS chlorophyll data. We analyzed daily SeaWiFS chlorophyll data in the central region of Wilkinson Basin (Stn A) (Fig. 1) from January 1, 1998 to December 12, 2004 to explore the interannual variability of fall phytoplankton blooms. The SeaWiFS data were obtained from NASA's Goddard Space Flight Center as Level 1 data and processed to daily Level 3 data at 1.1 km resolution using the OC4v4 algorithm (O'Reilly et al. 2001). To evaluate the quality of the satellite data, we compared the SeaWiFS data with *in situ* surface chlorophyll data from summertime survey data collected at the same time and locations (Fig. 1) for the years 1998, 2000, and 2001 (Townsend et al. 2001, 2005) when both satellite and *in situ* data were available.

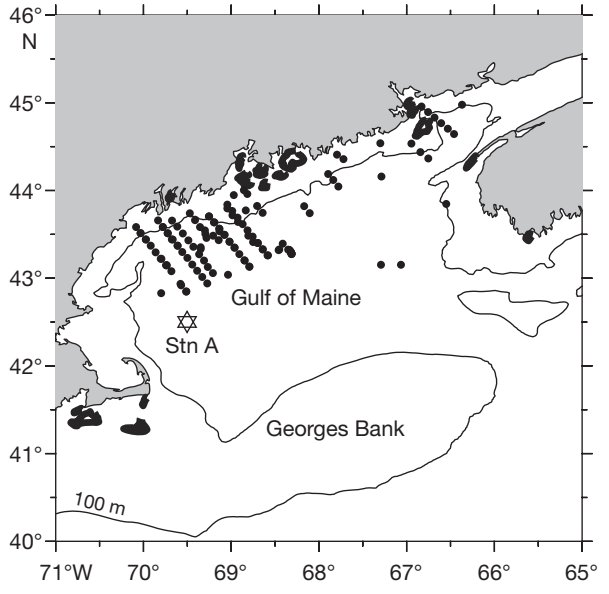

Fig. 1. The Gulf of Maine and Georges Bank regions. Black circles: matching points for comparisons between *in situ* measurements and SeaWiFS chlorophyll data; star: Stn A, located in the center of Wilkinson Basin

Box model setup. ***Mixed layer box biological models:*** The mixed-layer box model consists of a 2-layer system; an upper mixed layer in which all biological variables are vertically well mixed and a deep layer containing higher concentrations of nutrients. Between these 2 layers is a discontinuous interface that is defined as the mixed-layer depth. This conceptual mixed-layer model was described in detail in Chen (2002), who used it to examine responses of nutrient fluxes and the various biological compartments to changes in the upper mixed-layer depth.

For the simplest situation (N model), assuming that the upper, actively mixed layer contains no nutrients (nitrate), and the deep stratified layer contains an excess of nutrients, we can derive an N model equation as:

$$\frac{dN}{dt} = \frac{N_0 - N}{h}\frac{dh}{dt} \quad (1)$$

where N is the nutrient concentration in the mixed layer, N_0 the nutrient concentration in the deep layer, t the time and h the mixed-layer depth. Considering a 2-variable system with nutrients and phytoplankton, we can derive an NP box model in the form of:

$$\frac{dN}{dt} = \frac{-\int_{z=-h}^{0} f(I)dz}{h}\frac{V_m N}{K_s + N}P + \varepsilon_P P + \frac{N_0 - N}{h}\frac{dh}{dt} \quad (2)$$

$$\frac{dP}{dt} = \frac{\int_{z=-h}^{0} f(I)dz}{h}\frac{V_m N}{K_s + N}P - \varepsilon_P P - \frac{P}{h}\frac{dh}{dt} \quad (3)$$

where P is the phytoplankton concentration in the mixed layer, $f(I)$ the light function, z the depth, V_m the maximum growth rate for phytoplankton, K_s the half saturation constant for phytoplankton uptake, and ε_P the mortality rate of phytoplankton. In this box-model study, the light function is:

$$f(I) = I_0 e^{-K_{ext} z} \quad (4)$$

where I_0 is the light at the sea surface, K_{ext} the diffuse attenuation coefficient for irradiance, and z the depth below the sea surface. Self-shading (on K_{ext}) and seasonal variability of I_0 were not included in these studies.

Similarly, a 3-variable NPZ box model can be given as:

$$\frac{dN}{dt} = \frac{-\int_{z=-h}^{0} f(I)dz}{h}\frac{V_m N}{K_s + N}P + (1-\gamma)g_{max}\frac{P^2}{K_P^2 + P^2}Z + \varepsilon_P P + \varepsilon_Z Z^2 + \frac{N_0 - N}{h}\frac{dh}{dt} \quad (5)$$

$$\frac{dP}{dt} = \frac{\int_{z=-h}^{0} f(I)dz}{h}\frac{V_m N}{K_s + N}P - g_{max}\frac{P^2}{K_P^2 + P^2}Z - \varepsilon_P P - \frac{P}{h}\frac{dh}{dt} \quad (6)$$

$$\frac{dZ}{dt} = \gamma g_{max}\frac{P^2}{K_P^2 + P^2}Z - \varepsilon_Z Z^2 - \frac{Z}{h}\frac{dh}{dt} \quad (7)$$

where Z is the zooplankton concentration in the mixed layer, g_{max} the maximum grazing rate of zooplankton on phytoplankton, K_p the half saturation constant of zooplankton grazing on phytoplankton, ε_Z the mortality rate of zooplankton, and γ the zooplankton assimilation coefficient.

Using the same approach, we can derive a 4-variable NPZD box model given as:

$$\frac{dN}{dt} = \frac{-\int_{z=-h}^{0} f(I)dz}{h}\frac{V_m N}{K_s + N}P + \beta g_{max}\frac{P^2}{K_P^2 + P^2}Z + \varepsilon_D D + \frac{N_0 - N}{h}\frac{dh}{dt} \quad (8)$$

$$\frac{dP}{dt} = \frac{\int_{z=-h}^{0} f(I)dz}{h}\frac{V_m N}{K_s + N}P - g_{max}\frac{P^2}{K_P^2 + P^2}Z - \varepsilon_P P - \frac{P}{h}\frac{dh}{dt} \quad (9)$$

$$\frac{dZ}{dt} = \alpha g_{max}\frac{P^2}{K_P^2 + P^2}Z - \varepsilon_Z Z^2 - \frac{Z}{h}\frac{dh}{dt} \quad (10)$$

$$\frac{dD}{dt} = (1-\alpha-\beta)g_{max}\frac{P^2}{K_P^2 + P^2}Z + \varepsilon_P P + \lambda\varepsilon_Z Z^2 - \varepsilon_D D - \frac{D}{h}\frac{dh}{dt} \quad (11)$$

where D is the detritus concentration in the mixed layer, ε_D the detritus remineralization rate, α the zooplankton assimilation coefficient, β the zooplankton excretion coefficient, and λ the recycle coefficient of zooplankton loss term.

We used the Mellor-Yamada level-2.5 (MY-2.5) closure scheme (Mellor & Yamada 1982) to calculate the time sequences of mixed-layer depths via the turbulence mixing. The surface forcing used for this calculation was from the MM5 meteorological model-assimilated hindcast data at Stn A (Fig. 1) from September 1 to December 10 for each year. MM5 is a meso-scale meteorological model developed by Dudhia et al. (2003) and configured to the GoM by Chen et al. (2005).

Nitrogen is assumed to be the limiting nutrient for the fall bloom, which is usually dominated by smaller, non-diatom species (O'Reilly & Busch 1984). We integrated the models starting from August 31 in each instance. The response of P to N was examined for 3 situations: high, climatological average, and low nitrate conditions (hereafter referred to as Type-1, Type-2, and Type-3 initial conditions, respectively). This experiment was made with the understanding

that the nitrate concentration in the GoM can vary significantly over an interannual time scale (Townsend et al. 2006, Townsend & Ellis 2010). To construct the nutrient profile for these 3 conditions, we first defined a simple function of N in the form of:

$$\begin{cases} N(z) = 0, & -5\,\mathrm{m} \le z \le 0 \\ N(z) = \dfrac{N_{\max}(z+5)^2}{(z+5)^2 + z_0^2}, & z < -5\,\mathrm{m} \end{cases} \quad (12)$$

where $N_{\max}$ is the maximum value of the nitrate concentration at the bottom, z_0 the mid-depth parameter, and z the depth. Then we used Eq. (12) to fit the August climatological nitrate profile in the GoM (Fig. 2) to generate the Type-2 initial condition. The Type-1 and Type-3 initial conditions were created by increasing or decreasing $N_{\max}$ and z_0 in the deep layer of Eq. (12) (Fig. 2). The parameters of these fitted curves are listed in Table 1. Except for the situation designed to test the sensitivity of the initial nutrient conditions, the default initial nutrient profile (N_0) for all the cases was set as Type-2, and the initial nutrient concentrations in the upper mixed layer for the box model were set to zero. Initial conditions for each box model are detailed in Table 2 and biological parameters in Table 3.

To estimate the relative importance of each variable and parameter, we first non-dimensionalized the above equations by defining each variable as a product of its scale and a non-dimensional variable, such as

$$N = N_t N',\ N_0 = N_t N_0',\ t = \frac{t'}{V_m}\ P = N_t P',\ Z = N_t Z',\ D = N_t D',\ h = Hh'$$

where N_t is the total N in the vertical water column, V_m the maximal growth rate, H the total water depth, and N', N_0', P', Z', D', and h' are non-dimensional variables constrained between 0 and 1. The resulting equations (Appendix A) suggest the importance of the following variables and parameters in each model.

N model: Nitrate is used solely as a conservative tracer forced by the change in the mixed-layer depth.

NP model: Two parameters,

$$K_s' = \frac{K_s}{N_t} \text{ and } \varepsilon_p' = \frac{\varepsilon_p}{V_m}$$

occur in the non-dimensional NP equations and describe the scaled half saturation constant and scaled phytoplankton mortality rate. Numerical experiments were made to examine the sensitivity of K_s' and ε_p'.

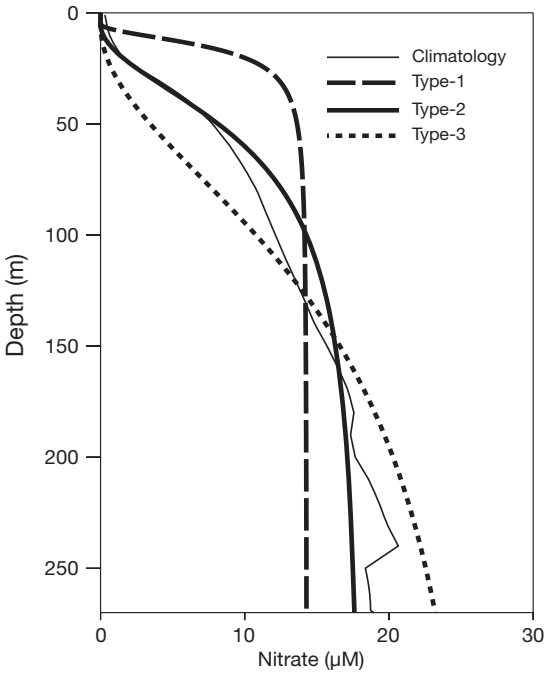

Fig. 2. Vertical nitrate profile for August climatology (mean of years) at Stn A. Type-1: high-nutrient conditions, Type-2: normal nutrient conditions; Type-3: low-nutrient conditions

Table 1. Parameters used for fitting curves of nitrate profiles (Eq. 12). $N_{\max}$: maximum value of the nitrate concentration at bottom; z_0: mid-depth parameter

Name	$N_{\max}$ (μM)	z_0 (m)
Type-1	14.3	10
Type-2	18.23	50
Type-3	27.96	120

Table 2. Descriptions for box model setup. N: nitrate, P: phytoplankton, Z: zoo plankton, D: detritus

Model name	Initial conditions	Forcing conditions
N model	Nitrate is set as 0 μM N in the upper layer and Type-2 (Fig. 2) in the lower layer	The driving forcing is the time series of the mixed-layer depth from Sep 1 to Dec 10 for each year (pre-calculated using MM5 surface forcing and MY-2.5 turbulence models). The light intensity at the sea surface is set as constant through out the simulation.
NP model	Nitrate is set as in the N model. The initial phytoplankton is set as 0.01 μM N in the upper layer and 0 μM N in the lower layer	
NPZ model	Nitrate is set as in the N model. The initial phytoplankton and zooplankton are set as 0.01 μM N in the upper layer and 0 μM N in the lower layer	
NPZD model	Nitrate is set as in the N model. The initial phytoplankton and zooplankton are set as 0.01 μM N in the upper layer and 0 μM N in the lower layer. The detritus is set as 0 μM N in both layers	

Table 3. Biological parameters used in NP, NPZ, and NPZD baseline models. N: nitrate, P: phytoplankton, Z: zooplankton, D: detritus

Symbol	Definition	Value	Unit
NP model			
V_m	Maximum phytoplankton growth rate	3.0	d^{-1}
K_s	Half saturation constant for phytoplankton uptake	0.5	μM N
ε_P	Phytoplankton mortality	0.1	d^{-1}
K_{ext}	Diffuse attenuation coefficient for irradiance	0.1	m^{-1}
NPZ model (the values of V_m, K_s, ε_P, K_{ext} are the same as those in the NP model)			
g_{max}	Maximum grazing rate of zooplankton on phytoplankton	0.3	d^{-1}
K_P	Half saturation constant of zooplankton grazing on phytoplankton	0.3	μM N
ε_Z	Zooplankton mortality	0.2	d^{-1}
γ	Zooplankton assimilation coefficient	0.3	Dimensionless
NPZD model (the values of V_m, K_s, ε_P, K_{ext}, g_{max}, K_P, ε_Z are the same as those in the NPZ model)			
α	Zooplankton assimilation coefficient	0.3	Dimensionless
β	Zooplankton excretion coefficient	0.3	Dimensionless
λ	Recycle coefficient of zooplankton loss term	0.7	Dimensionless
ε_D	Detritus remineralization rate	0.1	d^{-1}

NPZ model: Compared to the *NP* processes, there are 2 new non-dimensional parameters $g_{max}' = \frac{g_{max}}{V_m}$ and $K_P' = \frac{K_P}{N_t}$. These parameters control the growth of zooplankton, which were examined in the numerical experiments in comparison to the key parameters in the NP model.

NPZD model: The detritus equation consists of 'sloppy feeding' from zooplankton grazing, phytoplankton and zooplankton mortality, detritus remineralization, and loss due to the deepening of the mixed layer. Compared to NP and NPZ models, the mortalities of zooplankton and phytoplankton are the source of detritus, and the regenerated nutrients are produced by the detritus remineralization at the constant rate ε_D. The key difference in dynamics between the NPZD and the NPZ models is the export of nutrients via detritus sinking. We hypothesize that this may impact the duration and intensity of the fall bloom due to the availability of recycled nitrate in the euphotic zone. A series of numerical experiments were conducted to examine the sensitivity of ε_D' (the scaled remineralization coefficient).

1D physical-biological coupled model. The coupled model consists of a 1D FVCOM (Chen et al. 2003, 2006a,b) and a flexible biological module. The biological model and physical model are integrated at the same time step so that the mixing process of the biological compartments is resolved. As with the box model, we conducted FVCOM-N, FVCOM-NP and FVCOM-NPZD model simulations.

The physical model, FVCOM, is a prognostic, unstructured-grid, finite-volume, free-surface, 3D primitive equation coastal ocean circulation model (Chen et al. 2003, 2006a). The model incorporates the modified MY-2.5 as a default setup for the vertical mixing and was adapted to simulate 1D processes (Chen et al. 2006b). It was spatially configured with 6 identical triangles around a center node. The model had 100 uniform layers in the vertical, which produce a resolution of 2.65 m for a total water depth of 265 m at Stn A. The external barotropic and internal baroclinic time steps were 12 and 120 s for the physical model, and the biological model was integrated using the same internal time step as the physical model. The model was driven by M_2 (principal lunar semidiurnal constituent) tidal forcing, surface wind stress, and heat flux forcing, which were extracted at Stn A from the MM5 meteorological model. For each yearly simulation, the initial conditions for temperature (T) and salinity (S) were specified using the regional GoM and George Bank FVCOM output of mean T and S on August 31 at Stn A.

A turbulence closure scheme usually has a problem at a mixing cutoff, and a background mixing value is needed for a stratified water condition. The MY-2.5 closure scheme is built on a mixing cutoff at Richardson no. = 0.25. A background mixing value of 10^{-4} m^2 s^{-1} was specified in our experiment. This value was validated via the turbulence measurement data collected in the GoM (Chen & Beardsley 1998, Chen et al. 2003).

The 1D structure of the biological model was constructed using the FVCOM general biological module (GBM) described in Chen et al. (2006b), and the NPZD model used the same formulation as Ji et al. (2008a) (see Appendix B for details). For the FVCOM-N experiments, we forced the model with (1) surface heat flux alone and (2) both surface heat flux and wind stress to examine the roles of heat flux and wind stress in the mixed-layer deepening during the fall season. Unlike

in the box model, the surface light intensity used in the 1D models varies with time using the shortwave radiation time series at Stn A from the MM5 model (Chen et al. 2005). For the FVCOM-NPZD experiments, the initial condition for the nitrate concentration was specified as Type-2, and the initial conditions for phytoplankton, zooplankton, and detritus were specified as the small amount of 0.01 µMN (phytoplankton, zooplankton and detritus are measured in terms of nitrogen).

In addition to the surface heat flux, freshening effects were also examined in this study. Two processes were considered here: (1) the change of initial stratification due to freshening and (2) intermittent freshening-induced variability of stratification. The experiments were designed with an aim to understand how these 2 processes impact biological processes. In the first process study, we conducted FVCOM-NP model experiments using various S initial profiles that represent different stratifications. T was set as 10°C throughout the water column, and S at the surface and bottom were set as 31 and 35, 33 and 35, and 33.5 and 34.5 with corresponding Brunt-Väisälä frequencies of ~0.01, 0.007, and 0.005 s^{-1}, respectively. In the second process study, 4 cases were tested using the FVCOM-NP model. They are:

Case 1: The surface salinity boundary was set fresher over a 4 mo period from September 1 to December 10.

Case 2: The surface salinity boundary was set fresher over a 2 wk period from September 16 to 31.

Case 3: The surface salinity boundary was set fresher over a 2 wk period from October 16 to 30.

Case 4: The surface salinity boundary was set fresher over a 2 wk period from November 16 to 31.

In the 1D experiment, freshening was considered by setting the surface flux boundary condition of salinity as follows

$$\frac{K_Z}{H}\frac{\partial S}{\partial \sigma}\Big|_{\sigma=0} = 1.2 \times 10^{-5} \text{m s}^{-1} \quad (13)$$

where K_Z is the diffusivity coefficient, H the water depth, S the salinity, and σ the sigma layer. This salt boundary condition means that freshwater is added into the system at a constant flux at the surface of the water column. Assuming the surface mixed layer is ~30 m deep, this flux can decrease the mixed-layer salinity by ~0.5 in 15 d in the model.

RESULTS

SeaWiFS chlorophyll and wind data

The SeaWiFS data showed that the surface chlorophyll concentrations in the GoM exhibited strong interannual variability (Fig. 3). The comparison between SeaWiFS-derived daily chlorophyll data and *in situ* measurements for summer months showed a clear correlation with considerable scatter ($r^2 = 0.3$, $p < 0.001$). Due to heavy cloud coverage in the GoM, caution should be taken when using these SeaWiFS data to draw quantitative conclusions, particularly for the time period during which only a few clear images existed. For example, Fig. 3 shows a significant peak in the chlorophyll concentration (3.02 µg l^{-1}) on November 8, 2003. Since this peak was observed only in 1 image, and there were no images available close to that day, occurrence of a real fall bloom event is unlikely. Comparison with *in situ* measurement data during those years helped us exclude inconsistent individual data points in the SeaWiFS data.

The calibrated SeaWiFS data revealed that the fall phytoplankton biomass varied significantly over the period from 1998 to 2004. In 1998, the chlorophyll concentration was high in late fall (November 12 to December 4). The average concentration for adjacent days was 2.2 µg l^{-1} (shown as a bold black bar in Fig. 3a), with a maximum of 3.88 µg l^{-1} on November 24. In 1999, Hurricane Floyd passed over the region with values of wind stress reaching as high as ~1 N m^{-2} on September 17. Following the passage of the hurricane, a peak of chlorophyll concentration with an average value of ~1.6 µg l^{-1} appeared during September 15–27. The maximum chlorophyll concentration in the fall of 1999 was ~3.63 µg l^{-1}, occurring in November. Another immediate high peak with an average of ~2.58 µg l^{-1} was observed between October 24 and November 6 (Fig. 3b). In 2000, no particularly high chlorophyll concentrations were observed during the fall season (Fig. 3c). In 2001, relatively high values appeared in late October, when the average chlorophyll concentration was ~2.2 µg l^{-1} from October 19 to 30, and a maximum value of 3.27 µg l^{-1} was recorded on October 21 (Fig. 3d). In 2002, relatively high chlorophyll concentrations were found between October 10 and 20 (Fig. 3e). In 2003 and 2004, the chlorophyll concentrations remained at low levels throughout the fall, except for the high values on November 8, 2003 already mentioned (Fig. 3f,g).

In summary, the SeaWiFS data from 1998 to 2004 indicated that fall blooms can be classified into 3 categories: (1) a relatively small magnitude hurricane-induced bloom, (2) gradual but relatively long-lasting blooms, and (3) the absence of any noticeable bloom. The first 2 categories seemed closely relevant to changes in the surface meteorological forcing. To illustrate the impact of surface forcing on the interannual variability of the fall bloom, we present next the box and 1D model results. To avoid redundancy, we only present the model results for 3 yr that were typical of the 3 types of blooms: 1999, a hurricane year; 2001, a normal bloom year; and 2004, a non-bloom year.

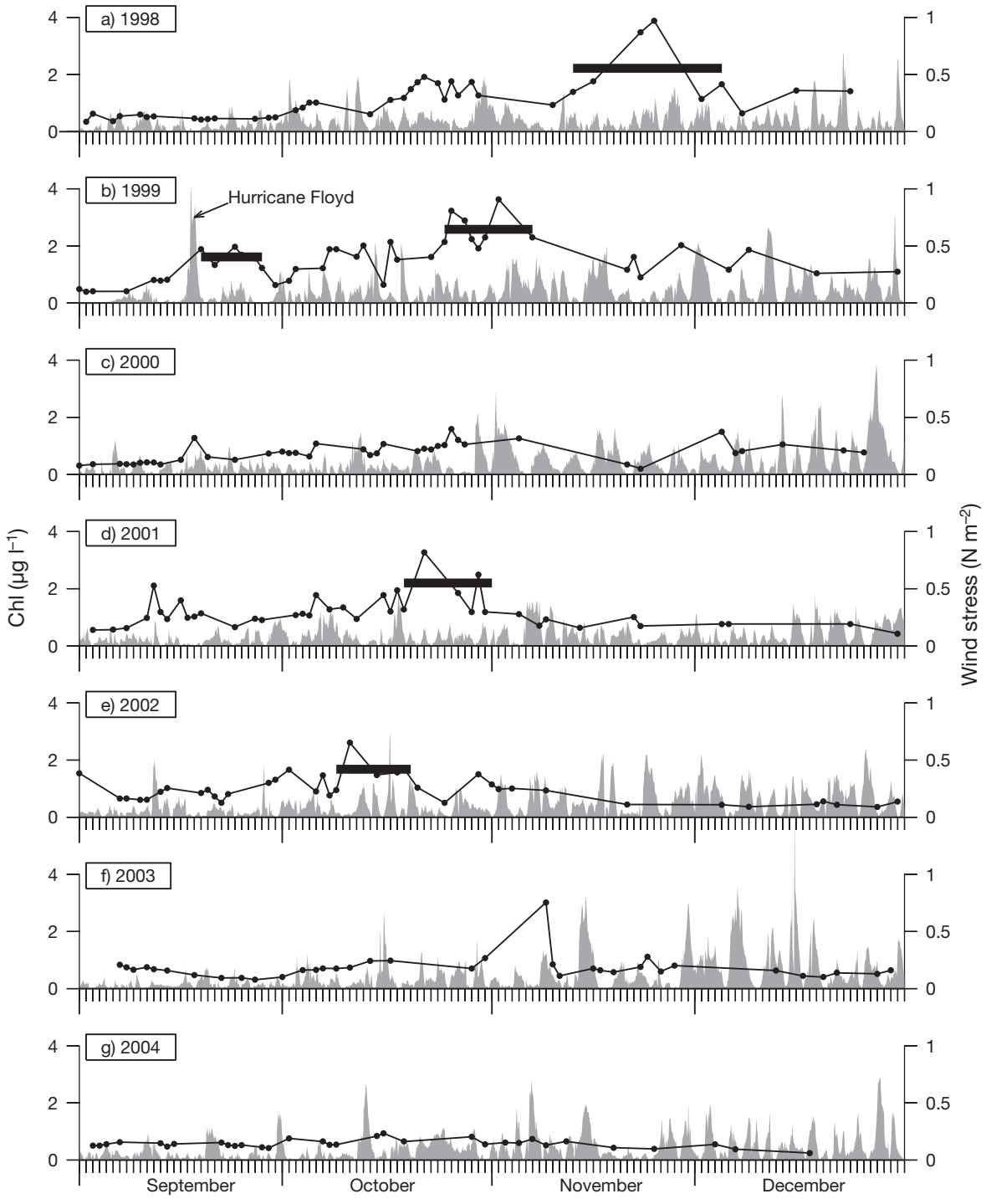

Fig. 3. Time series of SeaWiFS chlorophyll data (•) and wind stress data (grey-shaded areas) at Stn A for the years 1998 to 2004 (a–g). Tick marks represent days. Wind stress is based on MM5 meteorological model database. Bold black bars: averaged chlorophyll concentrations on adjacent days

Box model

The box model has a simplified structure for simulating the physical environment, thereby allowing a more tractable parameter analysis for the biological system. The model is driven by the change in mixed-layer depth computed based on the wind stress and net heat flux at the sea surface. The wind stress displayed an increasing tendency in magnitude with stochastic hurricane and storm events during the fall season

(Fig. 3). The net heat flux showed strong interannual variations as well. For example, accumulated heat loss from the ocean to the atmosphere from October to December was significantly greater in 1999 than in 2001 and 2004. Also the accumulated net heat flux was different between 2001 and 2004 during the period from September to October when the ocean was still warming up (the positive slope of accumulated net heat flux curve as shown in Fig. 4). These different surface forcings can generate considerable variations in the mixed layer on both short- and long-term scales, which, in turn, cause interannual variations in nutrient fluxes from the deep layer to the euphotic zone and consequently affect the fall bloom.

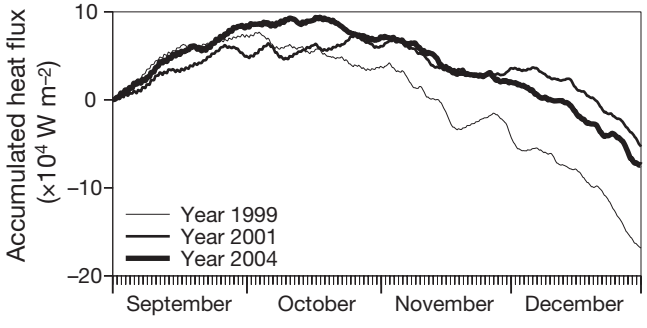

Fig. 4. Accumulated net heat flux at Stn A from September to December for 1999, 2001, and 2004. Tick marks represent days

N model runs

In 1999, the mixed-layer depth deepened rapidly from ~6 to ~30 m in the middle of September, immediately after the passage of Hurricane Floyd (Fig. 5a). After that, the mixed-layer depth retreated back to ~20 m in 2 to 5 d and then gradually deepened to about 60 m by the end of November, with a brief period of surface warming from November 20 to 25. During the same time period in 2001 and 2004, no hurricane or storm events occurred and the mixed-layer depth gradually deepened between September and December due to the seasonal increase of wind stress and cooling (Fig. 5b,c). The mixed layer in 2004 was generally deeper than in 2001, but shallower than in 1999. Consistent with the rapid deepening of the mixed layer, the largest vertical nitrate flux occurred in the middle of September 1999, reflected by an abrupt increase in nitrate concentration in the mixed layer (Fig. 5a). The normalized nitrate concentrations reached 0.54 by the end of 100 d of integration for 1999, 0.30 for 2001, and 0.35 for 2004, respectively

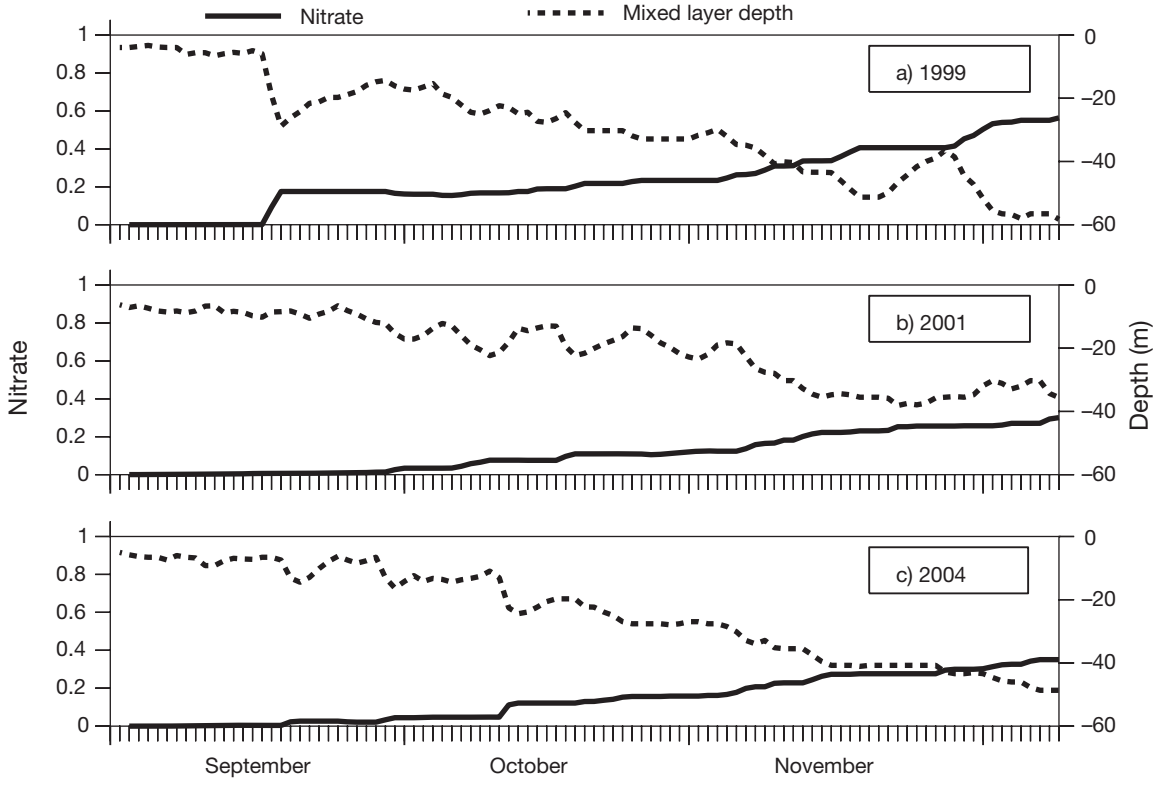

Fig. 5. Modeled mixed layer depths (dashed lines) and dimensionless nitrate concentrations (solid lines) in the mixed layer for the N model for years (a) 1999, (b) 2001, and (c) 2004. Tick marks represent days

(Fig. 5a–c). The results of the N model show that the vertical nitrate flux is proportional to the rate at which the mixed layer is deepening.

NP model runs

The NP box model successfully simulated phytoplankton responses to changes in the nitrate concentration resulting from surface forcing-induced deepening of the mixed-layer depth. Taking 1999 as an example, we can see that the normalized nitrate concentration in the upper mixed layer increased from 0 to ~0.2 during the hurricane period and then decreased to nearly 0 as a result of increased uptake by phytoplankton (Fig. 6a). Consequently, the phytoplankton biomass started to increase in the middle of September and reached approx. 0.2 to 0.5 by the end of the 100 d simulation. The initial increase of phytoplankton biomass following the hurricane appeared

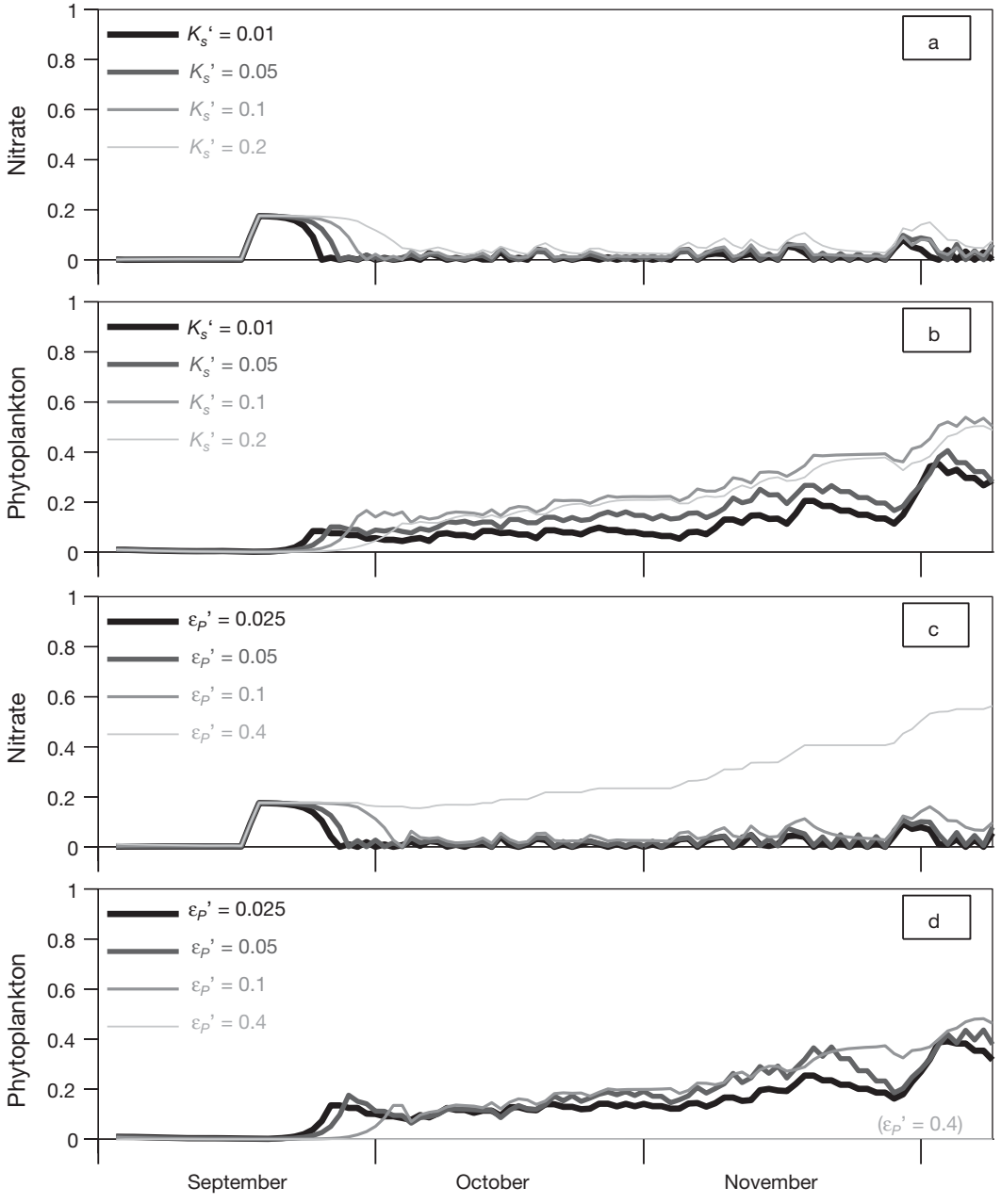

Fig. 6. Scaled nitrate and phytoplankton concentrations (dimesnionless) in the mixed layer predicted by the NP model using 2 sets of (a,b) scaled half saturation constant (K_s) and (c,d) scaled phytoplankton mortality (ε_P) for 1999

later, as K_s' became larger (Fig. 6b). Because the light used in this model is constant instead of seasonal, the phytoplankton biomass did not decrease by the end of December. To test the model sensitivity of the fall bloom to nutrient uptake and mortality rate of phytoplankton, sets of scaled half saturation constants K_s' (i.e. K_s/N_0) and normalized mortality rates ε_P' (i.e. ε_P/V_m) were tested in the NP model, while other parameters remained unchanged. For various values of K_s', the patterns of the time sequences of nitrate and phytoplankton concentrations were similar, but the total amount changed (Fig. 6a,b). For various values of ε_P', the results were similar except for the case in which ε_P' was as large as 0.4 (Fig. 6c,d). The phytoplankton in that case ceased to grow and the scaled nitrate concentrations continued to increase to about 0.54 over the 100 d integration period. This demonstrates that there is a threshold value for the normalized mortality rate of phytoplankton ε_P' (mortality rate divided by growth rate) that can prohibit the net growth of phytoplankton, and as a result the uptake of nitrate is limited. The results of the NP experiments indicate that the fall bloom can be triggered by vertical nitrate fluxes when the mortality of phytoplankton ε_P' is below a certain value and that the timing and magnitude of the fall bloom is related to nutrient influxes with both K_s' and ε_P'.

NPZ model runs

The general patterns of phytoplankton in the NPZ model runs were similar to those of the NP model predictions (data not shown). Since zooplankton was included in the biological compartments, we tested the sensitivity of the NPZ model to the scaled growth rate g_{max}' (0.03, 0.1, and 0.2 for each case) and K_P' (0.01, 0.03, and 0.05 for each case). We used the same phytoplankton mortality rate as that in the NP model so that we could explicitly examine the additional grazing factor brought about by the zooplankton component. The zooplankton concentrations increased as g_{max}' increased. The phytoplankton and nitrate concentrations, however, showed slight differences for various g_{max}' and K_P'. We also tested the initial condition of zooplankton grazing and found that there is a threshold value of initial zooplankton concentration that can inhibit the fall bloom, which behaves the same as the ε_P' threshold in the NP box model.

NPZD model runs

The most significant difference between NPZD and NPZ models is that the loss of phytoplankton and zooplankton is not directly converted back into nitrate. The detritus acts as a 'buffer' between the biological compartments and the nitrate, representing a more biologically realistic scenario. Over a realistic range of values for the scaled remineralization coefficient ε_D', the model reproduced a pattern similar to that from the NP and NPZ models (data not shown). The detritus concentrations increased as ε_D' decreased, and the phytoplankton concentrations decreased slightly as ε_D' decreased, but the general pattern remained unchanged.

NP model runs with different nitrate profiles

The nitrate concentrations in the deep water of the GoM varied significantly between years as a result of different deep-water mass types in the Gulf (Townsend et al. 2006, 2010, Townsend & Ellis 2010). To assess the influence of nitrate concentration in deep water on fall bloom dynamics, we repeated the NP model experiments using Type-1 (high nitrate) and Type-3 (low nitrate) profiles. The modeled phytoplankton was highly sensitive to the nutrient profiles. An example for 1999 is shown in Fig. 7. For the Type-1 profile, in which the nitrate concentration remained relatively high above 60 m water depth, a greater vertical nutrient flux was predicted, and the dimensionless nitrate concentration reached a maximum of 0.8. Correspondingly, the dimensionless phytoplankton concentrations reached 0.8 within ~7 d of the nitrate concentration peak and remained high for the rest of the simulation (Fig. 7a,b). For the Type-3 profile, in which the nitrate concentrations were low above 60 m water depth, the dimensionless nitrate concentration dropped to a minimum of 0.06. The corresponding phytoplankton concentrations were as low as 0.05 in September and October, and approx. 0.1 to 0.2 in November (Fig. 7c,d).

Given a fixed nitrate profile, all 4 box models (N, NP, NPZ, and NPZD) consistently reproduced fall blooms using a wide range of biological parameters, indicating that the mechanisms behind fall blooms are mainly controlled by the mixed-layer deepening and vertical nutrient fluxes, which have strong interannual variability due to the interannual variations in the surface forcing. The results also suggest that the dimensionless mortality rate of phytoplankton (ε_P') and the initial nutrient profile were important to the fall bloom initiation, while zooplankton grazing and remineralization processes were able to affect the overall intensity of fall blooms. The following 1D model results show more details regarding the importance of physical forcing related to mixed-layer deepening and surface nutrient replenishment.

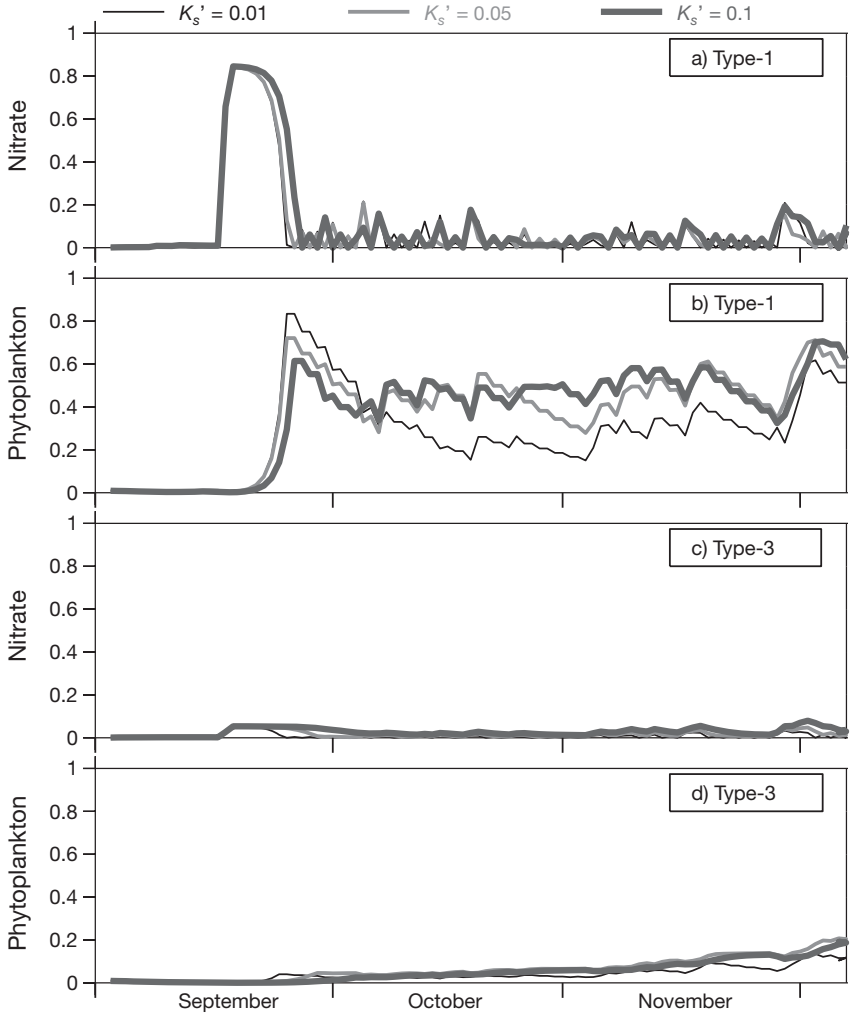

Fig. 7. Scaled nitrate and phytoplankton concentrations (dimensionless) in the mixed layer predicted by the NP model (a, b: using the Type-1 nitrate profile; c, d: using the Type-3 nitrate profile) for 1999. See Table 1 for profile types

1D Model

Wind stress and heat flux experiments

The 1D model has parameterization of vertical, continuous fluid hydrodynamics, which represents a more realistic approach than the box model for resolving the interactions among nutrients and biological components with a higher resolution in both temporal and spatial scales. To separate the influences of cooling and wind mixing, we ran the 1D FVCOM model forced by heat flux and wind stress as one case and the same model forced solely by heat flux as another case. The results show that cooling plays a key role in the dynamics of the upper mixed-layer depth during late fall, while the stochastic strong wind stress can contribute to the variability during early fall (as seen in 1999). For example, during the hurricane in 1999, the mixed-layer depth forced by both wind stress and heat flux reached ~30 m, and the nitrate concentrations in the mixed layer reached ~2.4 µM (Fig. 8a,b). When forced only by the heat flux, however, the mixed-layer depth was only ~8 m, and the nitrate concentrations in the mixed layer were ~1.1 µM (Fig. 8a,b). In late November of 1999 and 2001, when a weather system from the south or southwest region passed the GoM, the surface water was warmed for 1 to 2 wk. During that period, the intense winter wind was the key forcing to maintain the depth of the mixed layer (Fig. 8b–d). In 2001 and 2004, the modeled mixed-layer depth driven by heat flux only was slightly shallower than that predicted using both heat flux and wind stress, and the nitrate concentrations varied correspondingly (Fig. 8c–f), indicating that cooling was a dominant factor when intense wind events were absent. In general, the nutrients showed a gradually increasing tendency after the breakdown of the mixed layer with occasional disturbance by storms (Fig. 8a,c,e).

FVCOM-NPZD experiments

The FVCOM-NPZD model included variable light conditions, which generally decreased in strength. Thus, the critical depth (at which the vertical-integrated daily primary production generated by phtosynthesis process equals the vertical-integrated daily loss due to respiration) generally became shallow from September to December (Fig. 9a,g). For 1999, light became a limiting factor at the end of November when the mixed layer (~55 m) was deeper than the critical depth (~40 m) (Fig. 9a). The nitrate was initially stratified, while during the hurricane the nitrate was well mixed from the surface to a depth of ~30 m (Fig. 9a,b). After 2 to 5 d, the nitrate concentration became stratified again with the surface layer being depleted by phytoplankton uptake (Fig. 9b,c). From October to December, as the mixed layer deepened, the nitrate concentration in the mixed layer generally increased. The surface nitrate concentration increased from nearly 0 to 3.5 µMN by December (Fig. 9b,f), and the phytoplankton concentration changed correspondingly. From October to November, the phytoplankton biomass in the mixed layer remained at a high level of ~2 µMN until the end of November, when the mixed-layer depth

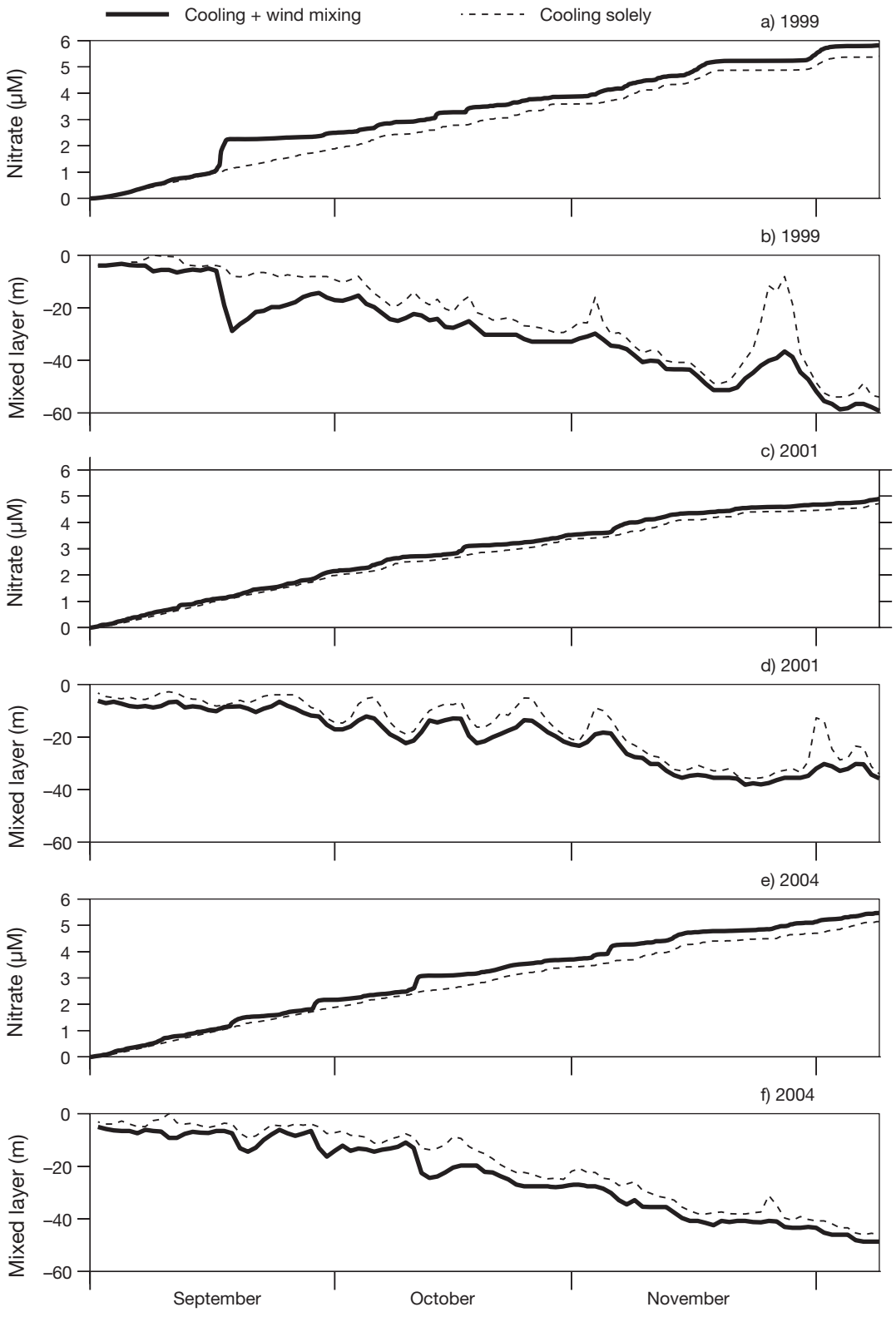

Fig. 8. Mixed-layer depths and nitrate concentrations in the surface mixed layer predicted by the FVCOM-N model for (a,b) 1999, (c,d) 2001, and (e,f) 2004. Dashed lines are the simulation forced solely by heat flux and solid lines forced by both heat flux and wind stress

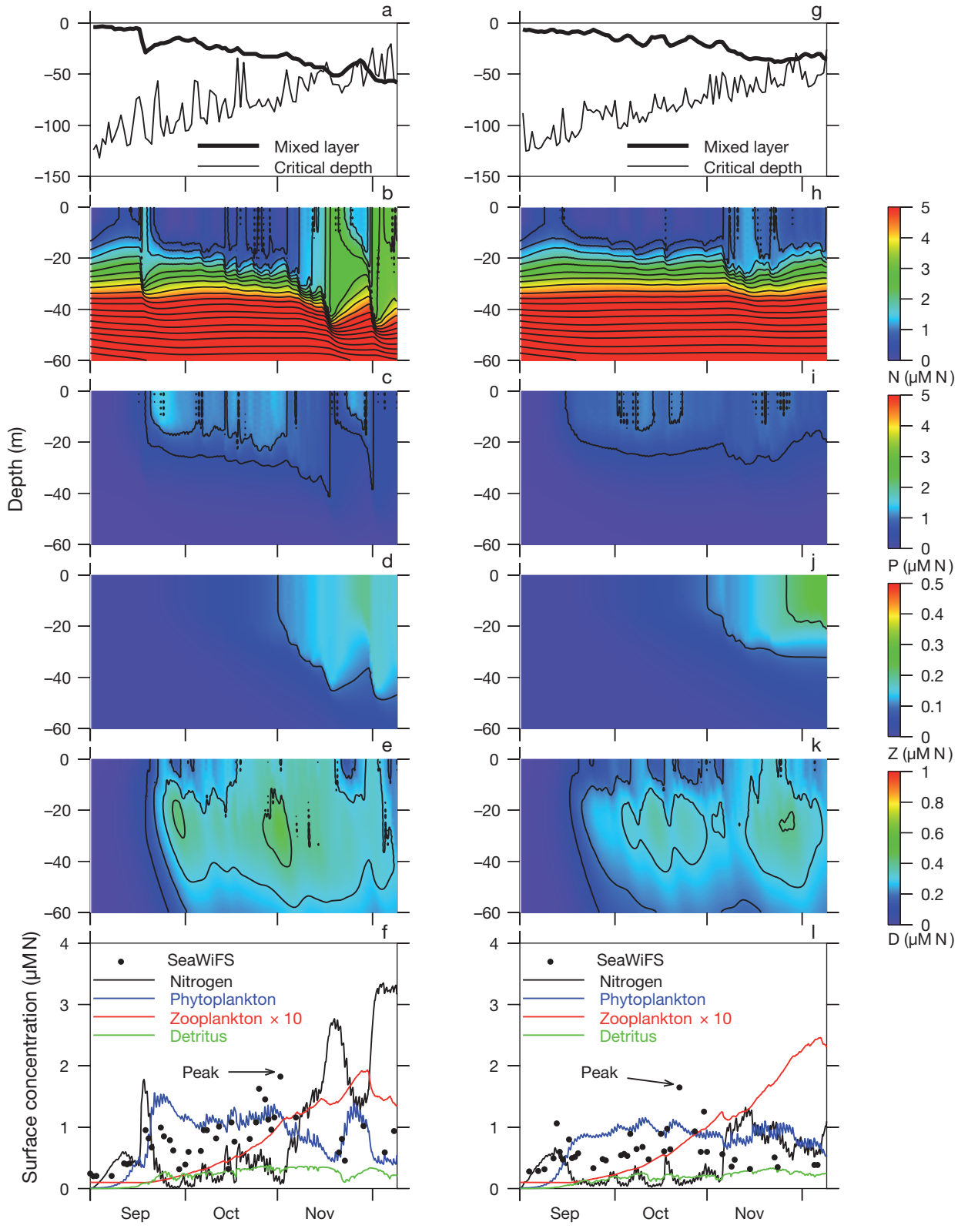

Fig. 9. (a,g) Mixed-layer depth and critical depth, and vertical profiles of (b,h) nitrate (N), (c, i) phytoplankton (P), (d,j) zooplankton (Z), and (e,k) detritus (D) for 1999 (left panels) and 2001 (right panels) predicted by the FVCOM-NPZD model. Comparison between SeaWiFS chlorophyll data and modeled surface biological concentrations for (f) 1999 and (l) 2001

reached ~45 m (Fig. 9c). At the end of November, the mixed-layer depth became shallow again for about 1 wk as a result of a net surface warming event (Fig. 9b). During that period, the phytoplankton concentration in the mixed layer increased, while the nitrate concentration decreased (Fig. 9b,c). By the end of November, the phytoplankton started to decrease, which was probably caused by 2 factors: (1) the reduced shortwave radiation in winter (light limitation) and (2) the deepening of the mixed layer due to strong cooling (Fig. 9a).

Although this is solely a process-oriented study of the fall bloom, and the biological initial conditions are set up for climatological conditions, the model successfully simulated the increase of the near-surface phytoplankton after the breakdown of the mixed layer in September. The increase of the modeled phytoplankton biomass started in the middle of September, consistent with the observed SeaWiFS data (Fig. 9f). The surface phytoplankton biomass remained at a high level during the fall, which was similar in magnitude to the SeaWiFS data until November, when the light became limiting and the mixed layer was much deeper. However, the model failed to capture some episodic bursts of surface phytoplankton such as the peak value of 1.9 µM on November 1, 1999 (Fig. 9f). There are certainly other physical and biological processes that have been ignored in our simple models. Even for our current models, we found that the failure to capture episode bursts was probably related to the parameterization used in the sink term of the detritus equation (Appendix B). Corresponding with the timing of the observed chlorophyll peak in the surface, the model predicted relatively high concentrations of detritus at ~30 m (Fig. 9e).

In 2001, the critical depth was deeper than the mixed layer for most of the simulation period (Fig. 9g). The simulation results for nitrate, phytoplankton, zooplankton, and detritus in 2001 (Fig. 9g–l) were very similar to those in 1999 (Fig. 9a–f). However, due to the absence of a hurricane in September and less cooling in 2001, phytoplankton, zooplankton, and detritus were generally less abundant than in 1999. The surface phytoplankton remained relatively abundant during the fall as observed in the SeaWiFS data, until November, when light became limiting, and the mixed layer was much deeper (Fig. 9i). Similar to the 1999 case, the phytoplankton peak value of 1.8 µM on October 21, 2001 was not reproduced (Fig. 9l).

Stratification and freshening experiments

For freshening, we tested the FVCOM-NP model for 1999 using 3 types of initial stratified conditions (Brunt-Väisälä frequencies of 0.005, 0.007, and 0.01 s^{-1}). It appeared that the initial stratification had little impact on the modeled phytoplankton concentrations in the mixed layer (data not shown). The modeled phytoplankton concentrations slightly decreased as the initial Brunt-Väisälä frequency was increased.

However, the timing of freshening and re-stratification seemed important to the variability of the fall bloom. Fig. 10 shows time sequences of surface phytoplankton concentration in the FVCOM-NP model by using the same initial conditions but adding freshwater through the diffusive flux using Eq. (13) for different periods (defined in Cases 1–4). For Case 1, the freshening strengthened the stratification and maintained higher phytoplankton abundance from September to December in all 3 yr with magnitudes of ~2 to 3 µM (shown as black line time series in Fig. 10). For the period October 16 to 30, we found that for 1999 and 2004 the differences between Case 2 (red line) and Case 3 (blue line) were significant, while for 2001, the differences in phytoplankton concentration among the tested cases were small until the end of October. The latter was because the mixed-layer depth in 2001 was shallower than in 1999 and 2004 during October due to the interannual variability in surface forcing. The freshening events in 2001 did not significantly change the mixed layer until November, while in 1999 and 2004, the mixed-layer depths were generally deeper than 20 m (Fig. 8b,f) during late October before the freshening events occurred. For Case 4, the freshening started in early winter, stratified the water, and greatly enhanced the phytoplankton. The model results indicate that in general, the intermittent freshening events increased the surface phytoplankton concentrations, especially when the mixed layer was deep enough to bring additional new nutrients before the freshening-induced events started re-stratification. Strong interannual variability can be generated depending on the combined effects of surface forcing and the timing and intensity of freshening events.

DISCUSSION

Causes of fall blooms on different time scales

A summary of the box model and 1D model results is given in Table 4. Using these models with surface forcing and idealized freshening events, we examined 3 major hypotheses: (1) the seasonal increase in vertical mixing leads to a gradual increase in phytoplankton biomass that persists throughout the fall; (2) hurricanes (or other strong wind events) lead to sudden vertical fluxes of nutrients into surface waters, which can trigger phytoplankton development, particularly when it is followed by re-stratification; and (3) intermittent freshening events can cause great variability in the timing and strength of the fall bloom.

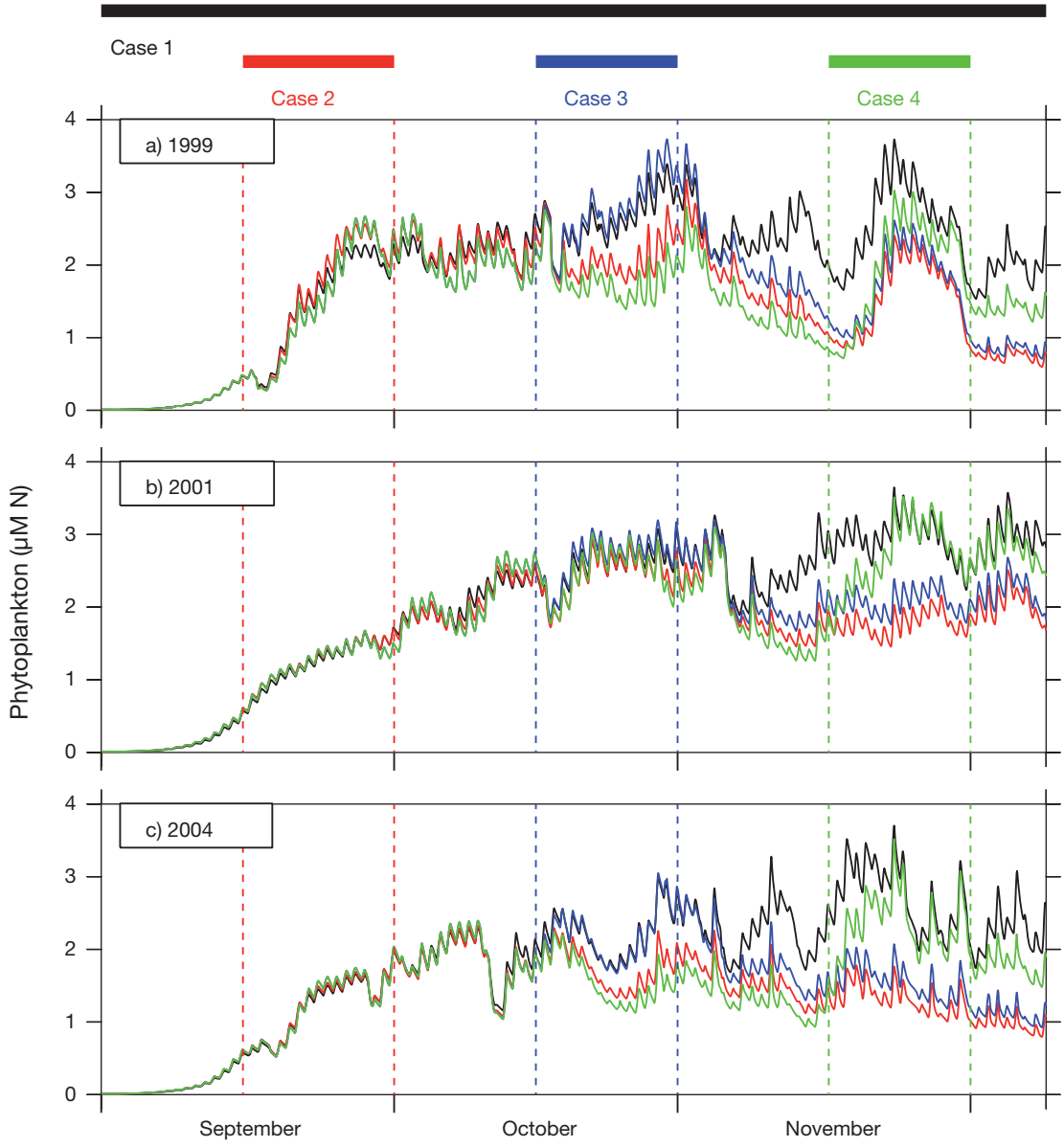

Fig. 10. Time sequences of modeled surface phytoplankton concentrations for freshening cases using the FVCOM-NP model for (a) 1999, (b) 2001, and (c) 2004. The black, red, blue and green bold lines on top indicate the timing of freshening (Case 1: Sep 1 to Dec 10, Case 2: Sep 16 to 31, Case 3: Oct 16 to 30, and Case 4: Nov 16 to 31)

For the first hypothesis, the NP, NPZ, and NPZD box models reproduced vertical nitrate fluxes from mixed-layer deepening and long-term fall blooms under a wide range of biological parameters. This result indicates that the simple concentration-based model is sufficiently robust to resolve the basic mechanism of the fall bloom. These models, however, failed to reproduce the decrease in phytoplankton in winter when light becomes limiting and the mixed layer continues to deepen. The 1D model captures the pattern where surface concentrations of phytoplankton increase from September to October and start to decrease at the end of October, and thus these results are consistent with our basic understanding of the fall bloom. That is, the deepening of the mixed layer in fall brings nutrients to the surface layer, where light is still sufficient for phytoplankton development.

For the second hypothesis, the NP, NPZ, and NPZD box models reproduced the quick nitrate increase during the intense vertical mixing that resulted from the hurricane. Since the nitrate flux was nearly proportional to the rate of mixed-layer deepening, the dramatic deepening of the mixed layer caused by this wind-mixing event created a significant nitrate flux into

Table 4. Summary of model results. N: nitrate, P: phytoplankton, Z: zooplankton, D: detritus, FVCOM: finite-volume community ocean model. Both box model and 1D model show that the physical forcing accounts for the response of fall bloom through short-term and long-term nutrient flux through changes in mixed-layer depth. For more specific details, the box model results show influences of the biological parameters such as phytoplankton mortality, zooplankton grazing rate, and remineralization rate. The 1D model, with more physical setting options, shows the impacts of physical factors such as wind stress versus heat flux, seasonal light variation, different initial stratification conditions, and intermittent freshening events. T: water temperature; *S*: salinity

	Box model			
Type	N model	NP model	NPZ model	NPZD model
Results	Surface forcing can cause interannual variability of nutrient influx on both short-term and long-term scales	Results are sensitive to the initial nutrient profile and the phyto-plankton-loss term. For 1999, a rapid increase of P appears after the passage of a hurricane	The zooplankton concentrations increase as the growth rate of zooplankton increases until phytoplankton mortality and zooplank-ton grazing inhibit the fall bloom	The remineralization rate does not change the general pattern of the fall bloom
	1D model			
Type	FVCOM-N	FVCOM-NPZD	FVCOM-NP	FVCOM-NP
Experiments	Different surface forcing (heat flux solely or heat flux plus wind stress)	Including seasonal light variation and all biological compart-ments	Different initial stratification conditions (*T*/*S*)	Different freshening periods
Results	Stochastic storms contribute to the variability during early fall as shown in 1999, while for late fall, all cases show that the heat flux is the domi-nant factor controlling the mixed layer depth. This variability of surface forcing leads to significant variability of nutrient flux	Models successfully simulate the timing of fall bloom and the decline of fall bloom due to the light limitation and deeper mixed layer. The magnitude of fall bloom is consistent with the observed values	Using different initial stratification conditions forced by the same surface forcing, the modeled surface phytoplankton concen-trations are similar in patterns and slightly change in the ampli-tudes	For intermittent freshening events (Cases 2–4), the results show that the combined effect of surface forcing and the timing of freshening can be significant for the interannual variability of fall bloom

the surface layer, where the nitrate was subsequently taken up by phytoplankton. During such wind events, vertical stratification is broken down, and nitrate concentration increases in the surface mixed layer. The rapid increase in phytoplankton followed the re-stratification of the upper water column ~2 to 5 d later. During the hurricane, the rapid deepening of the mixed layer immediately increased the nitrate concentrations at the surface but did not immediately trigger a phytoplankton bloom. Instead, only after the stratification was re-established did we see a phytoplankton response to the elevated nutrient concentration. The re-stratification usually occurs on a relatively short time scale.

For the third hypothesis, only the 1D model was employed, because vertical mixing dynamics are not explicitly included in the box model. The results indicate that the initial conditions of stratification and intermittent freshening events exert different effects on the fall bloom. It has been suggested that surface-water freshening in the Scotian Shelf and GoM region is related to the spring bloom dynamics (Ji et al. 2007). Also, freshening-induced stratification has been argued to lead to greater phytoplankton production in the fall, which might benefit the growth of smaller copepods (Greene & Pershing 2007).

We found that stronger initial stratification did not contribute to higher concentrations of phytoplankton. Under weaker initial stratification conditions, although more nutrients were brought up to the surface, a reduction in phytoplankton concentration was observed as a result of the dilution effect. However, the Cases 1–4 run with intermittent freshening events indicate that surface freshening, following a deep mixing with enhanced surface nutrient supply from the depth, can force a dynamic stratification process and promote phytoplankton growth. Caution needs to be taken when interpreting the intermittent freshening case, though. In reality, the fresher water that replaces high-nutrient and high-salinity surface water (due to strong preceding mixing) might have different (usually lower) nutrient concentrations, so its effect on phytoplankton growth enhancement could be diminished. A better

way to look at this case is, due to the enhanced freshening, the re-stratification after strong mixing occurs, and mixing of high-nutrient water from mid-depths with the low-nutrient surface water can still facilitate stronger phytoplankton growth.

Factors affecting surface mixing: heat flux versus surface wind

Among our hypotheses, seasonal variability in surface forcing is the dominant factor controlling the dynamics of the fall phytoplankton bloom. Extreme wind events such as a hurricane can only be significant over a relatively short period of time, and it is the re-stratification process that triggers an early fall bloom. However, such events do not significantly increase the accumulated biomass throughout the fall. The accumulated biomass is more strongly impacted by the seasonally accumulated effects of surface forcing (mostly by cooling during late fall).

We used the MY-2.5 turbulent closure scheme to compute the mixed-layer depth. Considering the uncertainties in these mixed-layer estimates, we repeated the numerical experiments using mixed-layer depths generated by the Price-Weller-Pinkel (PWP) model (Price et al. 1986), which calculates the mixed-layer depth based on static instability, mixed-layer instability, and shear-flow instability. The results show no significant changes in terms of bloom dynamics, suggesting that the model results are not sensitive to the differences of mixed-layer estimates between MY-2.5 and PWP models. However, both box model and 1D model results were sensitive to the initial nutrient concentrations, which only changed the magnitude of biological compartments, but had little effect on the general temporal variation.

Increasing complexity and bloom variability

Our approach in this study was to use models of increasing complexity in terms of modeled biological and physical processes. Findlay et al. (2006) used a simple system of parametrically forced ordinary differential equations to model the fall bloom in an open ocean ecosystem and reported that the rate of vertical mixing was important. They found that neither rapid nor gradual deepening of the mixed layer triggered a fall bloom; instead, a phytoplankton response required an intermediate mixing rate. However, the deepening rate of the mixed layer was simplified as a constant rate, and nutrient concentrations below the mixed layer were kept constant in their study. It is unclear how a system would respond if it had variable mixed-layer dynamics and nutrient concentrations. Compared to the Findlay et al. (2006) results, our model results suggest that besides the rate of deepening of the mixed layer, re-stratification dynamics after the break down of the mixed layer (hurricane case) and gradual deepening of the mixed layer can also trigger the accumulation of phytoplankton in the euphotic layer. The interannual variability can be largely explained by the surface forcing via controlling the nitrate flux, and fall blooms in coastal regions are significantly affected by the intermittent disturbances of wind mixing, cooling events and re-stratification.

According to Taylor & Mountain (2009), the interannual variability in surface salinity in the GoM can significantly affect the depth of vertical convective mixing in the GoM. Mupparapu & Brown (2002) compared the PWP model-simulated mixed-layer depths with measured mixed-layer depths and found that by excluding the role of convection, the PWP model underestimates the mixed-layer depth. At least 2 interesting questions can be raised concerning convection. First, how does vertical convection affect the fall bloom? Second, can the interannual variability of convection impact the spring bloom the following year by altering the surface nutrient concentrations in spring?

Another important factor, which the 1D model misses, is lateral advection. Lateral advection may bring nutrient-poor or -rich water into the GoM or affect the stratification with fresh or salty water, which can greatly change the fall bloom. Our 1D model analysis here consists of a process-oriented study. It helped us to shed new light on the impact of surface forcing on the fall bloom dynamics and interannual variations. Based on what we have learned from the box and 1D model experiments, a phytoplankton increase may be favored by the input of nutrient-rich water through lateral advection, which is analogous to an increased nutrient flux, or intermittent freshening with re-stratification following strong mixing as the low-salinity water encounters the high-salinity (high-nutrient) water from the deeper mixed layer. However, if the low-salinity water contains few nutrients, the situation will become more complicated by the combined effects of re-stratification and nutrient limitation.

Based on our results, the near-surface phytoplankton should increase with the entrainment of nutrients whenever the mixed layer depth deepens due to wind mixing and cooling. This result cannot be used to explain why there was no significant evidence of the fall bloom in 2000 and 2004, even though significant wind variability and cooling were observed. A further investigation on other physical and biological processes, such as phytoplankton response to light changes, nutrient recycling, and short-term variability of surface forcing, is needed.

CONCLUSIONS

The interannual variability of the fall bloom was examined first using the SeaWiFS satellite chlorophyll data in Wilkinson Basin in the western GoM. We found 3 general patterns in fall phytoplankton blooms: (1) a response to short-term perturbations such as a hurricane event that rapidly deepens the mixed layer and brings nutrients to the surface in early fall, or a freshening event that re-stratifies the mixed layer in later fall; (2) a response to gradual variation of the mixed layer such as the seasonally increasing wind mixing and cooling that gradually deepens the mixed layer; and (3) the absence of high chlorophyll concentrations throughout the fall. Possible factors controlling the interannual variability of fall blooms include surface forcing (wind mixing and heat flux), freshening, biological processes, convective mixing, and advection.

Using both box models and 1D models, we reproduced the increase in phytoplankton biomass in the fall when the surface mixed layer deepens, leading to changes in the nitrate influx. The box model results indicate that the intensity of phytoplankton is also sensitive to initial nutrient profiles and mortality of phytoplankton, but the dominant pattern is mostly caused by the dynamics of the mixed layer. The 1D model results reveal that the surface mixed-layer depth is controlled by both cooling-induced and wind-induced mixing during early fall, but particularly by cooling-induced mixing in late fall. The re-stratification process following the passage of a hurricane and seasonal, gradual deepening of the mixed layer can trigger phytoplankton development. The influence of freshening events is more complicated and depends on the timing of freshening events and nutrient content in the mixed layer. In general, the freshening events are important for the increase of the phytoplankton concentration during late fall when the mixed layer is deep enough to entrain additional nutrients. Further studies with a 3-dimensional model are required to resolve other factors (such as vertical and horizontal advection) that can potentially affect the fall bloom and were not resolved in the present study.

Acknowledgements. This research was supported by NOAA (grants NA04NMF4720332 and NA05NMF4721131) and a doctoral start-up fund by Shanghai Ocean University for S.H., the US GLOBEC Northwest Atlantic/Georges Bank Program through NSF grants (OCE-0234545, OCE-0227679, OCE-0606928, OCE-0712903, OCE-0732084, and OCE-0726851), NERACOOS, MWRA as well as MIT Sea Grant College Programs with grant nos. 2006-RC-103 and 2008-R/RC-107, NERACOOS and MWRA funds for C.C., NSF grant (OCE-0228943) to D.W.T., the WHOI Smith Chair in Coastal Oceanography and NOAA grant NA-17RJ1223 for R.C.B., and NSF (grant OCE-0727033) and NOAA (grant NA17RJ1223) to R.J. The experiments were conducted using the Linux clusters in the Marine Ecosystem Dynamics Modeling Laboratory at the School of Marine Science and Technology, University of Massachusetts-Dartmouth, funded by the SMAST Fishery Program through NOAA grants NA04NMF4720332 and NA05-NMF4721131. This paper is US GLOBEC contribution no. 700, 11-0101 in the SMAST Contribution Series, School of Marine Science and Technology, University of Massachusetts-Dartmouth. The work is also partially supported by the Shanghai Ocean University Program for International Cooperation (no. A-2302-10-0003), the Program of Science and Technology Commission of Shanghai Municipality (no. 09320503700), the Fund for Shanghai Excellent Youth Scholar (no. B-8101-09-0237) and the Leading Academic Discipline Project of Shanghai Municipal Education Commission (project no. J50702).

LITERATURE CITED

Bigelow HB (1926) Plankton of the offshore waters of the Gulf of Maine. Bull US Bur Fish 40:1–509

Chen C (2002) Marine ecosystem dynamics and modeling. Higher Education Press, Beijing (in Chinese)

Chen C, Beardsley RC (1998) Tidal mixing over finite-amplitude banks: a model study with application to Georges Bank. J Mar Res 56:1163–1203

Chen C, Liu H, Beardsley RC (2003) An unstructured, finite-volume, three-dimensional, primitive equation ocean model: application to coastal ocean and estuaries. J Atmos Ocean Technol 20:159–186

Chen C, Beardsley RC, Hu S, Xu Q, Lin H (2005) Using MM5 to hindcast the ocean surface forcing fields over the Gulf of Maine and Georges Bank region. J Atmos Ocean Technol 22:131–145

Chen C, Beardsley RC, Cowles G (2006a) An unstructured grid, finite-volume coastal ocean model (FVCOM) system. Oceanography 19(1):78–89

Chen C, Cowles G, Beardsley RC (2006b) An unstructured grid, finite volume coastal ocean model: FVCOM user manual, 2nd edn. SMAST/UMASSD Technical Report 06-0602, University of Massachusetts Datrmouth, North Dartmouth, MA

Dudhia J, Gill D, Manning K, Wang W, Bruyere C, Wilson J, Kelly S (2003) PSU/NCAR mesoscale modeling system tutorial class notes and user's guide. MM5 modeling system version 3, Mesoscale and Microscale Meteorology Division, National Center for Atmospheric Research, Boulder, CO

Findlay HS, Yool A, Nodale M, Pitchford JW (2006) Modelling of autumn plankton bloom dynamics. J Plankton Res 28: 209–220

Fogel ML, Aguilar C, Cuhel R, Hoolander DJ, Willey JD, Paerl HW (1999) Biological and isotopic changes in coastal waters induced by Hurricane Gordon. Limnol Oceanogr 44:1359–1369

Friedland KD, Hare JA, Wood GB, Col LA and others (2008) Does the fall phytoplankton bloom control recruitment of Georges Bank haddock, *Melanogrammus aeglefinus*, through parental condition? Can J Fish Aquat Sci 65: 1076–1086

Gran HH, Braarud T (1935) A quantitative study of the phytoplankton in the Bay of Fundy and the Gulf of Maine (including observations on hydrography, chemistry and turbidity). J Biol Board Can 1:279–467

Greene CH, Pershing AJ (2007) Climate drives sea change: Changes in Arctic climate have contributed to shifts in abundances and seasonal cycles of a variety of species in the northwest Atlantic. Science 315:1084–1095

Hitchcock GL, Smayda TJ (1977a) Bioassay of lower Narra-

gansett Bay waters during the 1972-1973 winter-spring bloom using the diatom *Skeletonema costatum*. Limnol Oceanogr 22:132–139

Hitchcock GL, Smayda TJ (1977b) The importance of light in the initiation of the 1972–1973 winter-spring diatom bloom in Narragansett Bay. Limnol Oceanogr 22:126–131

Ji R, Chen C, Franks PJS, Townsend DW and others (2006) Spring phytoplankton bloom and associated lower trophic level food web dynamics on Georges Bank: 1-D and 2-D model studies. Deep-Sea Res II 53:2656–2683

Ji R, Davis CS, Chen C, Townsend DW, Mountain DG, Beardsley RC (2007) Influence of ocean freshening on shelf phytoplankton dynamics. Geophys Res Lett 34: L24607 doi:10.1029/2007GL032010

Ji R, Davis C, Chen C, Beardsley RC (2008a) Influence of local and external processes on the annual nitrogen cycle and primary productivity on Georges Bank: a 3-D biological-physical modeling study. J Mar Syst 73:31–47

Ji R, Davis C, Chen C, Townsend D, Mountain D, Beardsley RC (2008b) Modeling the influence of low-salinity water inflow on winter-spring phytoplankton dynamics in the Nova Scotian Shelf-Gulf of Maine region. J Plankton Res 30:1399–1416

Mellor GL, Yamada T (1982) Development of a turbulence closure model for geophysical fluid problems. Rev Geophys Space Phys 20:851–875

Mupparapu P, Brown WS (2002) Role of convection in winter mixed layer formation in the Gulf of Maine, February 1987. J Geophys Res 107:3229 doi:10.1029/1999JC000116

O'Reilly JE, Busch DA (1984) Phytoplankton primary production on the northwestern Atlantic shelf. Rapp P-V Reùn Cons Int Explor Mer 183:255–268

O'Reilly JE, Maritorena S, Siegel DA, O'Brien MC and others (2001) Ocean color chlorophyll *a* algorithms for SeaWiFS, OC2 and OC4: version 4. In: Hooker SB, Firestone ER (eds) SeaWiFS Postlaunch Tech Rep Series, Vol 11. SeaWiFS postlaunch calibration and validation analyses: Part 3. NASA Tech. Memo. 2000-206892. NASA Goddard Space Flight Center, Greenbelt, MD, p 9–23

Price JF, Weller RA, Pinkel R (1986) Diurnal cycling: observations and models of the upper ocean response to diurnal heating, cooling and wind mixing. J Geophys Res 91: 8411–8427

Son S, Platt T, Fuentes-Yaco C, Bouman H, Devred E, Wu Y, Sathyendranath S (2007) Possible biogeochemical response to the passage of Hurricane Fabian observed by satellites. J Plankton Res 29:687–697

Taylor MH, Mountain DG (2009) The influence of surface layer salinity on wintertime convection in Wilkinson Basin, Gulf of Maine. Cont Shelf Res 29:433–444

Thomas AC, Townsend DW, Weatherbee R (2003) Satellite-measured phytoplankton variability in the Gulf of Maine. Cont Shelf Res 23:971–989

Townsend DW, Ellis WG (2010) Primary production and nutrient cycling on the Northwest Atlantic continental shelf. In: Liu KK, Atkinson L, Quiñones R, Talaue-McManus L (eds) Carbon and nutrient fluxes in continental margins: a global synthesis. IGBP Book Series. Springer-Verlag, Berlin, p 234–248

Townsend DW, Spinrad RW (1986) Early spring phytoplankton blooms in the Gulf of Maine. Cont Shelf Res 6:515–529

Townsend DW, Keller MD, Sieracki ME, Ackleson SG (1992) Spring phytoplankton blooms in the absence of vertical water column stability. Nature 360:59–62

Townsend DW, Cammen LM, Holligan PM, Campbell DE, Pettigrew NR (1994) Causes and consequences of variability in the timing of spring phytoplankton blooms. Deep-Sea Res 41:747–765

Townsend DW, Pettigrew NR, Thomas AC (2001) Offshore blooms of the red tide organism, *Alexandrium* sp., in the Gulf of Maine. Cont Shelf Res 21:347–369

Townsend DW, Pettigrew NR, Thomas AC (2005) On the nature of *Alexandrium fundyense* blooms in the Gulf of Maine. Deep-Sea Res II 52:2603–2630

Townsend DW, Thomas AC, Mayer LM, Thomas M, Quinlan J (2006) Oceanography of the northwest Atlantic continental shelf. In: Robinson AR, Brink KH (eds) The Sea, Vol 14. Harvard University Press, Cambridge, MA, p 119–168

Townsend DW, Rebuck ND, Thomas MA, Karp-Boss L, Gettings RM (2010) A changing nutrient regime in the Gulf of Maine. Cont Shelf Res 30:820–832

Appendix A. Non-dimensional box model equations

N model:

$$\frac{\mathrm{d}N'}{\mathrm{d}t'} = \frac{N_0' - N'}{h'}\frac{\mathrm{d}h'}{\mathrm{d}t'} \tag{A1}$$

NP model:

$$\frac{\mathrm{d}N'}{\mathrm{d}t'} = \frac{-\int_{z=-h}^{0} f(I)\mathrm{d}z}{H}\frac{N'}{K_s' + N'}\frac{P'}{h'} + \varepsilon_P' P' + \frac{N_0' - N'}{h'}\frac{\mathrm{d}h'}{\mathrm{d}t'} \tag{A2}$$

$$\frac{\mathrm{d}P'}{\mathrm{d}t'} = \frac{\int_{z=-h}^{0} f(I)\mathrm{d}z}{H}\frac{N'}{K_s' + N'}\frac{P'}{h'} - \varepsilon_P' P' - \frac{P'}{h'}\frac{\mathrm{d}h'}{\mathrm{d}t'} \tag{A3}$$

where $K_s' = \frac{K_s}{N_t}$, $\varepsilon_P' = \frac{\varepsilon_P}{V_m}$.

NPZ model:

$$\frac{\mathrm{d}N'}{\mathrm{d}t'} = \frac{-\int_{z=-h}^{0} f(I)\mathrm{d}z}{H}\frac{N'}{K_s' + N'}\frac{P'}{h'} + (1-\gamma) g_{\max}'\frac{(P')^2}{(K_P')^2 + (P')^2}Z' + \varepsilon_P' P' + m'(Z')^2 + \frac{N_0' - N'}{h'}\frac{\mathrm{d}h'}{\mathrm{d}t'} \tag{A4}$$

$$\frac{\mathrm{d}P'}{\mathrm{d}t'} = \frac{\int_{z=-h}^{0} f(I)\mathrm{d}z}{H}\frac{N'}{K_s' + N'}\frac{P'}{h'} - g_{\max}'\frac{(P')^2}{(K_P')^2 + (P')^2}Z' - \varepsilon_P' P' - \frac{P'}{h'}\frac{\mathrm{d}h'}{\mathrm{d}t'} \tag{A5}$$

$$\frac{\mathrm{d}Z'}{\mathrm{d}t'} = \gamma g_{\max}'\frac{(P')^2}{(K_P')^2 + (P')^2}Z' - m'(Z')^2 - \frac{Z'}{h'}\frac{\mathrm{d}h'}{\mathrm{d}t'} \tag{A6}$$

where $K_s' = \frac{K_s}{N_t}$, $\varepsilon_P' = \frac{\varepsilon_P}{V_m}$, $g_{\max}' = \frac{g_{\max}}{V_m}$, $K_P' = \frac{K_P}{N_t}$, $m' = \frac{m}{V_m}N_t$

NPZD model:

$$\frac{\mathrm{d}N'}{\mathrm{d}t'} = \frac{-\int_{z=-h}^{0} f(I)\mathrm{d}z}{H}\frac{N'}{K_s' + N'}\frac{P'}{h'} + \beta g_{\max}'\frac{(P')^2}{(K_P')^2 + (P')^2}Z' + \varepsilon_D' D' + \frac{N_0' - N'}{h'}\frac{\mathrm{d}h'}{\mathrm{d}t'} \tag{A7}$$

$$\frac{\mathrm{d}P'}{\mathrm{d}t'} = \frac{\int_{z=-h}^{0} f(I)\mathrm{d}z}{H}\frac{N'}{K_s' + N'}\frac{P'}{h'} - g_{\max}'\frac{(P')^2}{(K_P')^2 + (P')^2}Z' - \varepsilon_P' P' - \frac{P'}{h'}\frac{\mathrm{d}h'}{\mathrm{d}t'} \tag{A8}$$

$$\frac{\mathrm{d}Z'}{\mathrm{d}t'} = \alpha g_{\max}'\frac{(P')^2}{(K_P')^2 + (P')^2}Z' - m'(Z')^2 - \frac{Z'}{h'}\frac{\mathrm{d}h'}{\mathrm{d}t'} \tag{A9}$$

$$\frac{\mathrm{d}D'}{\mathrm{d}t'} = (1-\alpha-\beta) g_{\max}'\frac{(P')^2}{(K_P')^2 + (P')^2}Z' + \varepsilon_P' P' + \lambda m'(Z')^2 - \varepsilon_D' D' - \frac{D'}{h'}\frac{\mathrm{d}h'}{\mathrm{d}t'} \tag{A10}$$

where $K_s' = \frac{K_s}{N_t}$, $\varepsilon_P' = \frac{\varepsilon_P}{V_m}$, $g_{\max}' = \frac{g_{\max}}{V_m}$, $K_P' = \frac{K_P}{N_t}$, $m' = \frac{m}{V_m}N_t$, $\varepsilon_D' = \frac{\varepsilon_D}{V_m}$

Appendix B. 1D biological model

The biological equations are adapted from the NPZD model described in Ji et al. (2008a). Symbols *S1* to *S5* are used to represent different processes in controlling the source and sink terms of the biological state variables. *S1* is the nutrient uptake by phytoplankton, *S2* the zooplankton grazing on phytoplankton, *S3* the phytoplankton mortality, *S4* the remineralization of detritus, and *S5* the zooplankton mortality. These terms are defined as:

$$S1 = V_m \frac{N}{K_s + N}[(1 - e^{-\hat{\alpha}I})e^{-\hat{\beta}I}]P \quad \text{(B1)}$$

$$S2 = g_{\max} \frac{P^2}{K_p{}^2 + P^2} Z \quad \text{(B2)}$$

$$S3 = \varepsilon_p P \quad \text{(B3)}$$

$$S4 = \varepsilon_D D \quad \text{(B4)}$$

$$S5 = mZ^2 \quad \text{(B5)}$$

where N, P, Z, and D represent nitrogen, phytoplankton, zooplankton, and detritus concentrations, respectively.

For the FVCOM-N model, the change of nutrients over time can be described as

$$\frac{dN}{dt} = 0 \quad \text{(B6)}$$

For the FVCOM-NPZD model, the change of biological quantities over time can be described as:

$$\frac{\partial N}{\partial t} = -S1 + \beta S2 + S4 \quad \text{(B7)}$$

$$\frac{\partial P}{\partial t} = S1 - S2 - S3 \quad \text{(B8)}$$

$$\frac{\partial Z}{\partial t} = \alpha S2 - S5 \quad \text{(B9)}$$

$$\frac{\partial D}{\partial t} = (1 - \alpha - \beta)S2 + S3 - S4 + \gamma S5 \quad \text{(B10)}$$

The intensity of photosynthetically active radiation (PAR) at each depth is a function of the surface PAR and the light attenuation profile (including self-shading) and is described as

$$I(z) = I_0 \exp\left(-a_w z - a_p \int_{-z}^{0} P\,dz - a_D \int_{-z}^{0} D\,dz\right) \quad \text{(B11)}$$

where $I(z)$ is PAR at depth z, I_0 is surface irradiance, and a_w, a_P, and a_D are the light attenuation coefficients for pure water, phytoplankton, and detritus. For phytoplankton and detritus, the sinking terms,

$$-w_P \frac{\partial P}{\partial z} \text{ and } -w_D \frac{\partial D}{\partial z},$$

were added into Eqs. (B8) and (B10), respectively, in the studies.

For the FVCOM-NP model, the change of biological quantities over time can be described as:

$$\frac{\partial N}{\partial t} = -S1 + S3 \quad \text{(B12)}$$

$$\frac{\partial P}{\partial t} = S1 - S3 \quad \text{(B13)}$$

Table B1. Parameters used in the FVCOM-NPZD model

Symbol	Definition	Value	Unit
V_m	Maximum phytoplankton growth rate	2	d^{-1}
K_s	Half saturation constant for phytoplankton uptake	1	μMN
ε_P	Phytoplankton mortality	0.1	d^{-1}
$g_{\max}$	Maximum grazing rate of zooplankton on phytoplankton	0.3	d^{-1}
K_p	Half saturation constant of zooplankton grazing on phytoplankton	0.3	μMN
ε_Z	Zooplankton mortality	0.2	d^{-1}
α	Zooplankton assimilation coefficient	0.3	Dimensionless
β	Zooplankton excretion coefficient	0.3	Dimensionless
γ	Recycle coefficient of zooplankton-loss term	0.7	Dimensionless
ε_D	Detritus remineralization rate	0.1	d^{-1}
$\hat{\alpha}$	Light function coefficient	0.025	μMN s^{-1} W^{-1}
$\hat{\beta}$	Photoinhibition coefficient	0.001	μMN s^{-1} W^{-1}
w_p	Sinking velocity of phytoplankton	1	m d^{-1}
w_D	Sinking velocity of detritus	5	m d^{-1}

Table B2. Parameters used in the FVCOM-NP model

Symbol	Definition	Value	Unit
V_m	Maximum phytoplankton growth rate	2	d^{-1}
K_s	Half saturation constant for phytoplankton uptake	1	μMN
ε_P	Phytoplankton mortality	0.1	d^{-1}
$\hat{\alpha}$	Light function coefficient	0.025	μMN s^{-1} W^{-1}
$\hat{\beta}$	Photoinhibition coefficient	0.001	μMN s^{-1} W^{-1}
w_p	Sinking velocity of phytoplankton	1	m d^{-1}

Editorial responsibility: Alain Vézina, Dartmouth, Nova Scotia, Canada

Submitted: November 20, 2008; Accepted: January 18, 2011
Proofs received from author(s): March 25, 2011